Appl. Phys. B (2015) 121:179–185
DOI 10.1007/s00340-015-6215-9

Applied Physics B
Lasers and Optics

A fast algorithm to predict spectral broadening in CW bidirectionally pumped high-power Yb-doped fiber lasers

Áron Szabó[1,2] · Zoltán Várallyay[2,3] · Andrea Rosales-Garcia[4] · Clifford Headley[4]

Received: 21 May 2015 / Accepted: 1 September 2015 / Published online: 19 September 2015

Abstract A detailed, fast-converging iterative numerical method has been developed to model continuous-wave bidirectionally pumped Yb-doped fiber lasers with output powers of several hundred watts. The analysis shows nonlinearity-induced broadening of the lasing spectrum, which also modifies power efficiency. Cavity dynamics is described by combining the effects of Kerr nonlinearities with power evolution equations and rate equations. The fast method to find steady-state solutions for cavity setups is based on setting the temporal phase evolution as a stochastic process with proper spectral filtering. Spectral properties of bidirectionally pumped lasers are calculated within few minutes using a commercial desktop computer, and very good agreement with experimental measurements is obtained for up to 922 W total pump and 708 W output power.

1 Introduction

In the past 20 years, Yb-doped fiber lasers have been proven to be successful candidates to achieve record output powers in continuous-wave (CW) operation while maintaining high beam quality, due to their inherent advantages. Among others, high achievable dopant concentration results in increased gain and particularly small quantum defect makes possible low thermal load and the concept of tandem pumping (see [1] and references therein). These devices were theoretically shown to have the potential output powers of tens of kilowatts [2], and 100 kW has recently been demonstrated experimentally using a fiber combining technique [3]. At high-power or for long-cavity fiber lasers, fiber nonlinearities become important, acting on spatial and temporal properties of the output and consequently modifying its spectral properties. The effect of nonlinear-induced spectral broadening has already been investigated for ultra-long Raman fiber lasers with cavity lengths of up to 82.4 km and maximum output powers with near 1 W [4]. The reduced effective reflectivity of the fiber Bragg gratings caused by spectral broadening beyond the reflection spectra of the Bragg gratings leads to decreased power efficiency. In the case of Raman fiber lasers, several different models have been developed to describe the Kerr-induced broadening of the spectrum. A semiempirical approach to four-wave mixing has been used [5]. Fully analytical descriptions based on the wave turbulence approach [6, 7] and a modified shooting method combining the nonlinear Schrödinger equation (NLSE) and the steady-state power evolution equations [8] have also been demonstrated.

Kerr-induced spectral broadening of partially coherent (PC) CW beams has already been studied numerically in both the anomalous and normal dispersion regime of a fiber [9, 10] by handling the temporal evolution of the initial phase as a suitable stochastic process. Yb-doped fibers are generally used in the normal dispersion regime, and a proper adaption of PC beam modeling to predict spectral properties of CW Yb-doped fiber lasers would be useful.

✉ Áron Szabó
szabo.aron@tmit.bme.hu

[1] Department of Telecommunications and Media Informatics, Budapest University of Technology and Economics, Magyar tudósok körútja 2, Budapest 1117, Hungary

[2] ELI-ALPS, ELI-Hu Nonprofit Ltd., Dugonics tér 13, Szeged 6720, Hungary

[3] Furukawa Electric Institute of Technology Ltd., Vasgolyó utca 2-4, Budapest 1158, Hungary

[4] OFS Laboratories, 19 Schoolhouse Road, Suite 105, Somerset, NJ 08873, USA

An analytical model [11] successfully predicted secant-hyperbolic spectral shape of Yb-doped fiber lasers with output powers in the 1–12 W range and spectral widths below 0.1 nm by consequently neglecting dispersive phase shifts between the oscillating longitudinal modes. A quantitative numerical analysis was recently published by Turitsyn et al. [12] to explain the nonlinear spectral broadening and its consequences. The detailed numerical model was based on the combined NLSE, power evolution equations and effective two-level rate equations. The intensity and population distributions along the fiber were iteratively calculated assuming an effective propagation along an optical line with periodic cavity elements. Unidirectional pumping was assumed in the configuration. The approach was proven to be suitable for output powers of up to 12 W and for 35 m cavity length with proper high-performance computing facility. However, modeling such lasers with orders of magnitudes higher power and bidirectional pumping can result in computational issues arising from the accurate calculation of nonlinearities.

Here, we introduce a fast-converging iterative numerical method to investigate nonlinear cavity dynamics in bidirectionally pumped high-power CW Yb-doped fiber lasers with output powers of several hundred watts. We present details and further results of the algorithm summarized in Ref. [13]. The calculated results are in very good agreement with experiments for up to 708 W output power. The model is based on the combined NLSE, power evolution equations and rate equations. Forward and backward propagating CW laser beams are assumed to be spectrally filtered PC beams with additional one-photon-per-mode noise. The initial parameters of the beams are introduced into the doped fiber and then subject to the iteration process. Frosz's experimentally proven concepts [14] are the output of a CW pump laser for supercontinuum generation can be successfully modeled by a spectrally filtered phase diffusion process with additional one-photon-per-mode noise. This paper extends Frosz's concepts by finding the proper iteration for the spectral filtering of the phase diffusion process to successfully predict output spectra of high-power CW fiber lasers, while maintaining computing times (the order of minutes) on a commercial desktop computer.

2 Experimental setup

Figure 1 shows the experimental setup of the investigated Yb-doped cladding-pumped oscillator. For bidirectional pumping, OFS tapered fiber bundles (TFBs) are used which are suitable for coupling 18 multimode high-power sources and 1 single-mode signal source into the gain fiber. The high-power sources are 976 nm 25 W multimode laser diodes, each coupled into a 105/125 μm (core/cladding) diameter pigtail fiber to achieve up to 460 W pump power from both directions. Model validation was performed using a comparison of measured and calculated output powers and output spectra for a wide range of pump powers. The reflection spectra for both the high-reflection fiber Bragg grating (HR) and the output coupler (OC) are measured and are well approximated by proper Gaussian functions. These spectra are centered around 1070.1 nm with spectral FWHMs of 3.2 and 0.7 nm and peak reflections of 99.5 and 9.8 %, respectively. A 20-m length of Yb-doped fiber with cladding absorption of 0.8 dB/m at 915 nm is used as the gain fiber.

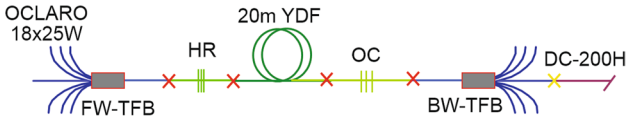

Fig. 1 Experimental setup for validation

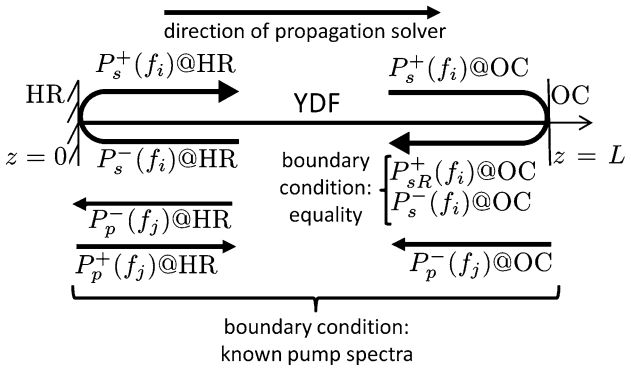

Fig. 2 Notations at the boundaries

3 Algorithm and validation

Our algorithm calculates the output power and spectral distribution of the CW laser over three different stages of calculations. The relevant pump and signal waves at the boundaries used for iterations or as fixed boundary conditions are summarized in Fig. 2, while the overview of the model is shown in Fig. 3. Within each stage, different calculation methods and boundary conditions are used to derive the approximate spectral power distribution, from an initial approximation in Stage 1 until a more accurate one in Stage 3. The core of the algorithm for every calculation stage is a propagation solver described below in detail, which is executed from the HR toward the OC numerous times until the calculated spectrum reaches an accuracy threshold of the current stage. The calculated power and spectrum in Stage 3 is the overall output of the algorithm.

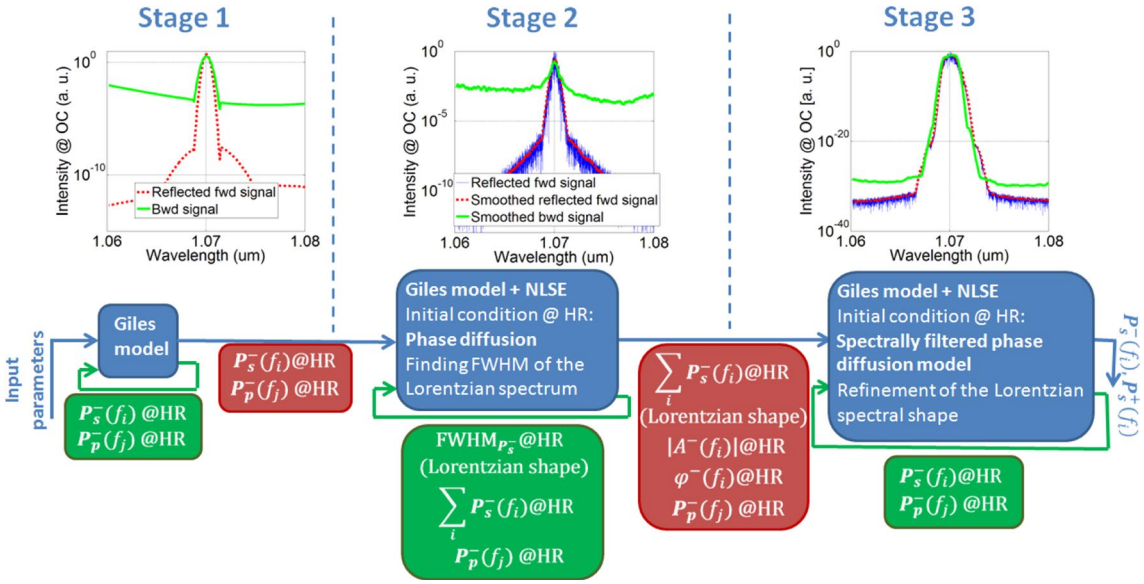

Fig. 3 Model overview

The direction of the propagation solver from the HR toward the OC is defined as being *forward*. The propagation distance, z, is considered positive in the forward direction. In all stages, the propagation solver handles the coupled forward and backward propagating signals and pumps together.

At the beginning of each iteration step within a stage, the spectral power of the backward propagating signal is iteratively set at the HR via multiplying by a proper signal feedback function (FF_{s}):

$$P^{-}_{\mathrm{s},n}(f_i)@\mathrm{HR} = P^{-}_{\mathrm{s},n-1}(f_i)@\mathrm{HR} \times FF_{\mathrm{s},n-1}(f_i) \tag{1}$$

where n represents the nth iteration step; s denotes the signal; and f_i is the ith frequency component. From the $P^{-}_{\mathrm{s},n}(f_i)$ @HR iterated backward signal, the forward signal $P^{+}_{\mathrm{s},n}(f_i)$ @HR is calculated using the wavelength dependent reflectivity of the HR. $+$ and $-$ signs denote forward and backward propagating waves, respectively. $FF_{\mathrm{s},n-1}(f_i)$ is calculated at the previous $(\mathrm{n}-1)$th step, after executing the propagator until the OC and obtaining backward $P^{-}_{\mathrm{s},n-1}(f_i)$ @OC and reflected forward $P^{+}_{\mathrm{sR},n-1}(f_i)$@OC signals at $z = L$. The latter was calculated from the forward signal $P^{+}_{\mathrm{s},n-1}(f_i)$@OC at the output coupler using the wavelength dependent reflectivity of the OC, similarly to the HR side. In the $(\mathrm{n}-1)$th iteration step, according to the boundary condition at the OC, the calculated spectra of $P^{-}_{\mathrm{s},n-1}(f_i)$@OC and $P^{+}_{\mathrm{sR},n-1}(f_i)$@OC should be equal with perfect initial conditions at $z = 0$. Consequently, the key task of each stage is finding the optimal signal feedback function which allows the accurate calculation of the forward and backward signals at $z = 0$ according to Eq. (1). After executing the nonlinear propagator, these signals satisfy the equality boundary condition with a predefined accuracy at $z = L$ as shown in Fig. 2.

The spectral components of the backward pump at the HR are also iterated by a suitable method, in order to match the boundary condition at the OC given by the known spectrum of the coupled backward pump. While the same iteration method for the backward pump proved to be useful for each stage, the form of $FF_{\mathrm{s},n}(f_i)$ to iterate the backward signal spectrum is changed in every stage and will be discussed later. Measured pump spectra were used as input for the calculations within every stage of the algorithm. The iteration of the backward pump is based upon the shooting method [15] for each spectral component. Equation (2) shows the heuristic approximate relationship between the HR and OC pump powers at the $(\mathrm{n}-1)$th and $(\mathrm{n}-2)$th iteration steps and the real spectrum of the backward pump, $P^{-}_{\mathrm{p}}(f_j)$. This approximation is valid when the pump is not depleted and the pump absorption is not saturated at any frequency:

$$\begin{aligned}&\frac{P^{-}_{\mathrm{p},n-1}(f_j)@\mathrm{OC} - P^{-}_{\mathrm{p}}(f_j)@\mathrm{OC}}{P^{-}_{\mathrm{p},n-2}(f_j)@\mathrm{OC} - P^{-}_{\mathrm{p}}(f_j)@\mathrm{OC}}\\ &\approx \frac{P^{-}_{\mathrm{p},n-1}(f_j)@\mathrm{HR} - P^{-}_{\mathrm{p}}(f_j)@\mathrm{HR}}{P^{-}_{\mathrm{p},n-2}(f_j)@\mathrm{HR} - P^{-}_{\mathrm{p}}(f_j)@\mathrm{HR}}\end{aligned} \tag{2}$$

Approximating the real spectrum of $P^{-}_{\mathrm{p}}(f_j)@\mathrm{HR}$ by the power at the nth iteration step denoted by $P^{-}_{\mathrm{p},n}(f_j)@\mathrm{HR}$, from Eq. (2) we obtain:

$$P^{-}_{\mathrm{p},n}(f_j)@\mathrm{HR} = \frac{\begin{aligned}&P^{-}_{\mathrm{p},n-2}(f_j)@\mathrm{HR} \times \Delta P^{-}_{\mathrm{p},n-1}(f_j)@\mathrm{OC}\\ &-P^{-}_{\mathrm{p},n-1}(f_j)@\mathrm{HR} \times \Delta P^{-}_{\mathrm{p},n-2}(f_j)@\mathrm{OC}\end{aligned}}{\Delta P^{-}_{\mathrm{p},n-1}(f_j)@\mathrm{OC} - \Delta P^{-}_{\mathrm{p},n-2}(f_j)@\mathrm{OC}} \tag{3}$$

In Eq. (3), the difference between the real spectral components of the backward pump at the output coupler and those obtained by any kth iteration step is denoted by $\Delta P^{-}_{\mathrm{p},k}(f_j)$@OC and stands for the following:

$$\Delta P^{-}_{\mathrm{p},k}(f_j)@\mathrm{OC} = P^{-}_{\mathrm{p},k}(f_j)@\mathrm{OC} - P^{-}_{\mathrm{p}}(f_j)@\mathrm{OC} \tag{4}$$

The iteration of the backward pump shown in Eq. (3) is valid in every stage of the algorithm.

In Stage 1, the propagation in the Yb-doped fiber neglects any dispersive and nonlinear effects and is restricted to the amplification of the spectral components of the electric field in the Yb-doped medium. The model used in this stage is based upon the effective overlap integral approximation of Giles et al. [16]. Power evolution equations for the frequency-dependent signals and pumps for a given nth iteration step have the form of

$$\begin{aligned}\frac{\mathrm{d}}{\mathrm{d}z}{P_{\mathrm{s},n}}^{\pm}(f_i) &= \mp\alpha_{\mathrm{s}}{P_{\mathrm{s},n}}^{\pm}(f_i) \\ &\pm (n_2\sigma_{e\mathrm{s}}(f_i) - n_1\sigma_{a\mathrm{s}}(f_i))\Gamma_s C{P_{\mathrm{s},n}}^{\pm}(f_i)\end{aligned} \tag{5}$$

$$\begin{aligned}\frac{\mathrm{d}}{\mathrm{d}z}{P_{\mathrm{p},n}}^{\pm}(f_j) &= \mp\alpha_{\mathrm{p}}{P_{\mathrm{p},n}}^{\pm}(f_j) \\ &\pm \left(n_2\sigma_{e\mathrm{p}}(f_j) - n_1\sigma_{a\mathrm{p}}(f_j)\right)\Gamma_p C{P_{\mathrm{p},n}}^{\pm}(f_j)\end{aligned} \tag{6}$$

where n_2 and n_1 are the upper- and lower-state populations, σ_e and σ_a are the frequency-dependent emission and absorption cross sections, respectively, and C is dopant concentration. For the core mode of the signal, the overlap factor is determined by a mode solver, while the pump overlap was obtained from preliminary measurement of the small signal loss of the propagating light in the cladding. This resulted in $\Gamma_s = 0.65$ and $\Gamma_p = 0.0038$ for the signal and the cladding pump, respectively. Stationary population inversion is assumed at each point of the fiber as the duration of a single round-trip in the present oscillator length is over three orders of magnitude smaller than the Yb lifetime [12], considered 2.3 ms. The coupled power evolution equations for the forward and backward propagating signals and pumps are solved from $z = 0$ (HR) toward $z = L$ (OC) by a four-step Runge–Kutta method [15]. When the total pump power is >400 W, the signals are spectrally resolved in a 20-nm-wide window in each stage. For lower pump powers, 12-nm-wide window ensures a stable convergence of the overall algorithm. In each iteration step of Stage 1, the feedback function $FF_{\mathrm{s},n}(f_i) \equiv FF_{\mathrm{s},n}$ is frequency independent and is calculated the following way:

$$\begin{aligned}FF_{\mathrm{s},n} &= 1 \\ &- B\left(\sum_i P^{+}_{\mathrm{sR},n}(f_i)@\mathrm{OC} - \sum_i P^{-}_{\mathrm{s},n}(f_i)@\mathrm{OC}\right),\end{aligned} \tag{7}$$

which equals 1 when the calculated backward and reflected forward signals have equal power at the output coupler. B is a suitable constant chosen to speed up the iteration. As Stage 1 calculates approximate signal powers and does not consider nonlinear spectral broadening, the $P^{-}_{\mathrm{s},n}(f_i)$@HR components assumed to have the same spectral shape that the reflectivity of the OC at the beginning of any nth iteration step. Accordingly, the output of Stage 1 following its final iteration step is the *total* backward signal power of $\sum_i P^{-}_{\mathrm{s}}(f_i)$@HR with an assumed spectral shape together with the spectral power distribution of the backward pump: $P^{-}_{\mathrm{p}}(f_i)$@HR.

The aim of Stage 2 is to provide a rough estimation of the real spectral shape of the backward signal $P^{-}_{\mathrm{s}}(f_i)$@HR by a Lorentzian function before executing the propagation solver. This is achieved by applying the phase diffusion model [17] i. e., the temporal phase evolution of the backward signal follows a Wiener process at the HR. According to Ref. [17], the FWHM of the resulting Lorentzian spectral shape is proportional to the variance parameter of the Wiener process, which makes possible to tune the spectral width of the signal at the beginning of each iteration step. One-photon-per-mode noise is also added to the spectrum [14]. The propagation solver in Stage 2 is based upon the NLSE involving second-order dispersion and self-phase modulation terms [18] with an additional gain term used to model the laser amplification in the nonlinear gain media for both the forward and backward propagating signals:

$$\frac{\partial A^{\pm}}{\partial z} = \left(\frac{\bar{+}i\beta_2}{2}\frac{\partial^2}{\partial T^2} \pm i\gamma\left|A^{\pm}\right|^2 \pm g(A^{+},A^{-})\right)A^{\pm} \tag{8}$$

Here, $A(z, T)$ denotes the slowly varying complex envelope and the signs stand for the forward and backward propagating signals, similarly to Stage 1. The number of sampling points of the spectral and temporal window is increased to 4096 for an accurate execution of the symmetric split-step Fourier method [18]. The equations for A^{+} and A^{-} are coupled via the gain term $g(A^{+},A^{-})$, which is determined numerically using the power evolution Eqs. (5)–(6), similarly to Stage 1. In this stage, Eqs. (5)–(6) are solved for 20 sequential segments within each split-step segment using the Runge–Kutta method. This subdivision is a trade-off to achieve increased accuracy of the gain calculation while keeping the computing time of the gain in the same order of magnitude of the dispersion and nonlinearity. The second-order dispersion and the nonlinear parameter are defined as $\beta_2 = 40\ \mathrm{ps}^2/\mathrm{km}$ and $\gamma = 0.003\ \mathrm{W}^{-1}\mathrm{m}^{-1}$, respectively. In this stage, the iteration of the backward pump and two signal iterations are executed simultaneously. The frequency-independent feedback function FF_{s} is calculated in

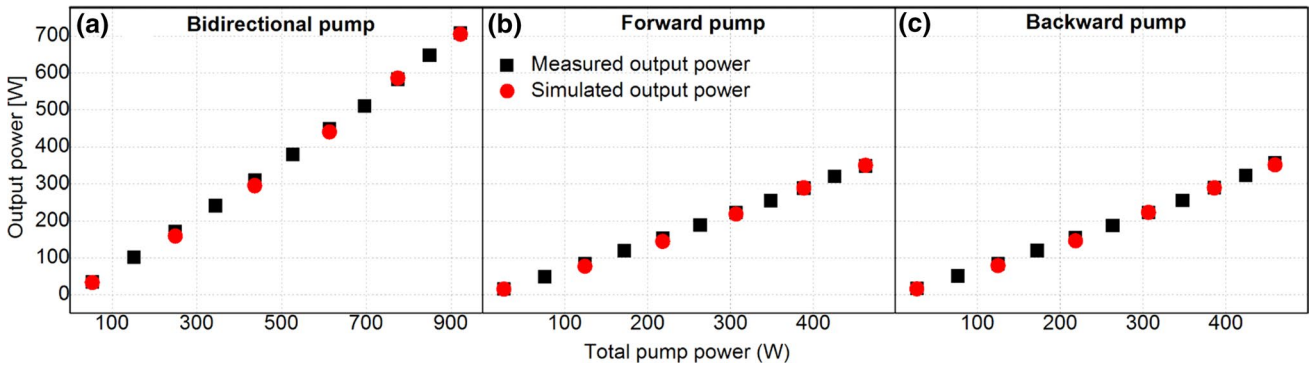

Fig. 4 Calculated and measured output powers as a function the total pump power for **a** bidirectional, **b** forward and **c** backward pumping

the same way as in Stage 1, while the spectral FWHM of $P_s^-(f_i)$@HR is scaled in each iteration step as follows:

$$FWHM_{P_{s,n}^-}\text{@HR} = FWHM_{P_{s,n-1}^-}\text{@HR} \times \frac{FWHM_{\left[P_{s,n-1}^-\right]_{MA}}\text{@OC}}{FWHM_{\left[P_{sR,n-1}^+\right]_{MA}}\text{@OC}} \quad (9)$$

In Eq. (9), the FWHM terms at the HR are set by the variance parameter of the Wiener process. The iteration process of Eq. (9) uses obtained spectral FWHM values at the OC calculated within each iteration step following the propagation. It is not possible to calculate FWHM of the noisy spectrum for a single realization of the Wiener process after propagating in the doped fiber so signal spectral curves are smoothed by a moving average for 50 points before the FWHM calculation, denoted by MA. Consequently, the outputs of Stage 2 are the spectral distribution of the backward pump power $P_s^-(f_j)$@HR, the total backward signal power $\sum_i P_s^-(f_i)$@HR and also the assumed Lorentzian spectral shape of the backward signal at the HR with the iterated spectral FWHM. The latter is involved implicitly in the complex spectral amplitude $|A^-(f_i)|$@HR and phase $\phi^-(f_i)$@HR at the output of Stage 2 as shown in Fig. 3.

The aim of Stage 3 is to use the $FF_s(f_i)$ to refine the calculated Lorentzian spectrum from Stage 2 via iterative spectral filtering. In this stage, we generalize Frosz's concepts [14] of spectral filtering the output of a phase diffusion model to obtain the measured laser spectra. We have shown that the output spectrum of a high-power CW Yb-doped fiber laser can be predicted by filtering the output spectrum of a phase diffusion model by a proper function calculated iteratively at the HR and then solving the NLSE, power evolution equations and rate equations from this iterated spectrum, until the OC. The feedback function $FF_s(f_i)$ defined by Eq. (1) is calculated from the obtained spectral power values at the OC following the propagation, using the heuristic expression:

$$FF_{s,n}(f_i) \sim \exp[K \times (1 - P_{sR,n}^+(f_i)_{MA}\text{@OC}/P_{s,n}^-(f_i)_{MA}\text{@OC})] \quad (10)$$

where MA is the moving average similarly to Stage 2. As this expression contains smoothed, broadened spectra at the OC, it has to be rescaled before the application of the feedback function to the initial signal spectrum at the HR, denoted by $\sim$. The exponential dependence ensures convergence of the spectral components at the OC boundary on a logarithmic scale if the parameter K is set properly. As the aim of the overall algorithm is to predict both the output spectral shape and power, the iterative spectral shaping in Stage 3 is allowed to fine-tune the total power. A deviation of <10 % was typical compared to the output of Stage 2. This fine-tuning of the output power proved to be crucial in achieving such good agreement with experiments.

The validation of the model was executed for forward, backward and bidirectional pumping schemes, with pump powers of up to 460 W in a single direction. Output signal powers as functions of the pump powers are shown in Fig. 4, while comparison of measured and calculated spectra are shown in Fig. 5. The calculated data show very good agreement with measurements, with deviation from the measured data below 8 % and below 10 % for the output powers and for the RMS spectral widths, respectively. The calculations were executed on a 8-core Intel Xeon X5450@3.00 GHz desktop computer with 16 GB RAM, and computation times for all scenarios, including high pump power regimes, were within 5 min. This is a reduction of over 1 order of magnitude of computing time compared with the resonator model based on the effective propagation in an optical line [12]. The decreased computing time is valid even with increased number of computations within a single propagation along the doped fiber compared to Ref. [12]. This increase in computations results from the subdivision of the split-step segments into Runge–Kutta segments for the numerical computation of the gain and

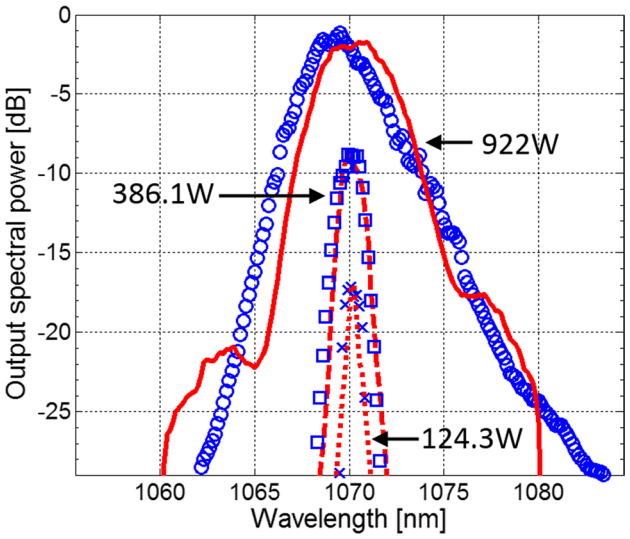

Fig. 5 Calculated (*lines*) and measured (*markers*) spectral powers with pump powers: 922 W bidirectional pump power (*solid line with circles*), 386.1 W backward pump with no forward pump (*dashed line with squares*) and 124.3 W forward pump with no backward pump (*dotted line with crosses*)

also considering the wavelength dependence of the absorption and emission cross sections. The inclusion of this wavelength dependence in the numerical solutions of the inversion level and gain in our model results in increased accuracy especially for significant spectral broadening.

We have found the form of $FF_s(f_i)$ is independent of the pump power in the investigated domain and independent of the fiber length for up to 40 m, while $0 < K < 1.5$. However, the exact dependence of K on the model parameters is still unresolved and needs further research.

We note that a well-established model for spectral broadening in Raman fiber lasers exists [6, 7], based on four-wave mixing between the large number of longitudinal modes which is described by the wave turbulence approach. Adaption and implementation of this method to the presented algorithm may allow further improvement in the speed of computation which is a component of future research.

The slightly asymmetrical broadening of the measured spectrum observed in Fig. 5 for the highest power indicates stimulated Raman scattering (SRS) similarly to Ref. [19]. According to Ref. [20] and considering 11 μm mode field diameter and 5 dB/km attenuation of the used fiber, the Raman threshold is approximately 1 kW, close to the highest output power in the present study. Above the threshold, the power scalability of CW fiber lasers and master oscillator power amplifier setups may be limited by SRS, although doped fibers with large mode area are preferentially used to suppress this effect [19, 21]. SRS dominates over stimulated Brillouin scattering for spectral bandwidths above 0.5 GHz [22], which is completely satisfied in the present case. Accordingly, SRS has a negligible effect in the investigated power domain but needs to be implemented when powers above 1 kW are used.

4 Conclusion

We have introduced a fast numerical method to predict nonlinear spectral broadening and output power in bidirectionally pumped high-power CW Yb-doped fiber lasers with output powers of several hundred watts. Calculation results were obtained within few minutes using a commercial desktop computer and show very good agreement with experiments for up to 708 W output power. The method can be considered as an adaption of Frosz's spectrally filtered phase diffusion concept [14] into high-power Yb-doped fiber lasers. The developed method makes possible to predict output spectral properties of high-power CW fiber lasers in a reasonable time without the need of extreme computational capacity.

Acknowledgments The ELI-ALPS project (GOP-1.1.1-12/B-2012-0001, GINOP-2.3.6-15-2015-00001) is supported by the European Union and co-financed by the European Regional Development Fund.

References

1. D. Richardson, J. Nilsson, W. Clarkson, J. Opt. Soc. Am. B **27**, B63 (2010)
2. J. Zhu, P. Zhou, Y. Ma, X. Xu, Z. Liu, Opt. Exp. **19**, 18645 (2011)
3. V. Fomin, V. Gapontsev, E. Shcherbakov, A. Abramov, A. Ferin, D. Mochalov, *100 kW CW Fiber Laser for Industrial Applications*. in Laser Optics International Conference (2014)
4. V. Karalekas, J. Ania-Castañón, P. Harper, S. Babin, E. Podivilov, S. Turitsyn, Opt. Exp. **15**, 16690 (2007)
5. J.-C. Bouteiller, IEEE Photon. Technol. Lett. **15**, 1698 (2003)
6. S. Babin, D. Churkin, A. Ismagulov, S. Kablukov, E. Podivilov, Opt. Lett. **31**, 3007 (2006)
7. S. Babin, D. Churkin, A. Ismagulov, S. Kablukov, E. Podivilov, J. Opt. Soc. Am. B **24**, 1729 (2007)
8. J. Hagen, R. Engelbrecht, O. Welzel, A. Siekiera, B. Schmauss, IEEE Photon. Technol. Lett. **19**, 1759 (2007)
9. A. Mussot, E. Lantz, H. Maillotte, T. Sylvestre, C. Finot, S. Pitois, Opt. Exp. **12**, 2838 (2004)
10. B. Barviau, S. Randoux, P. Suret, Opt. Lett. **31**, 1696 (2006)
11. S. Kablukov, E. Zlobina, E. Podivilov, S. Babin, Opt. Lett. **37**, 2508 (2012)
12. S. Turitsyn, A. Bednyakova, M. Fedoruk, A. Latkin, A. Fotiadi, A. Kurkov, E. Sholokhov, Opt. Exp. **19**, 8394 (2011)
13. Á. Szabó, Z. Várallyay, A. Rosales-Garcia, C. Headley, *CLEO: 2014, OSA Technical Digest*. Paper JTu4A.62
14. M. Frosz, Opt. Exp. **18**, 14778 (2010)
15. W.H. Press, S.A. Teukolsky, W.T. Vetterling, B.P. Flannery, *Numerical Recipies, the Art of Scientific Computing* (Cambridge University Press, Cambridge, 2007)
16. C.R. Giles, E. Desurvire, J. Lightw. Technol. **9**, 271 (1991)

17. M. Lax, Phys. Rev. **160**, 290 (1967)
18. G.P. Agrawal, *Nonlinear Fiber Optics* (Elsevier Science, Amsterdam, 2012)
19. A. Rosales-Garcia, H. Tobioka, K. Abedin, H. Dong, Z. Várallyay, Á. Szabó, T. Taunay, S. Sullivan, C. Headley, in *Proceedings of SPIE 9344, Fiber Lasers XII: Technology, Systems, and Applications, 93441G* (2015)
20. C. Jauregui, J. Limpert, A. Tünnermann, in *Proceedings of SPIE 7914, Fiber Lasers VIII: Technology, Systems, and Applications, 791408* (2011)
21. Y. Xiao, F. Brunet, M. Kanskar, M. Faucher, A. Wetter, N. Holehouse, Opt. Express **20**, 3296 (2012)
22. J. Limpert, F. Roser, S. Klingebiel, T. Scheriber, C. Wirth, T. Peschel, R. Eberhardt, A. Tünnermann, IEEE J. Sel. Top. Quantum Electron. **13**, 537 (2007)